Influence of Isolation Gap Size on the Collapse Performance of Seismically Base-Isolated Buildings

Zhe Qu,[a)] M.EERI, Shoichi Kishiki,[b)] Toshiyuki Nakazawa[c)]

Pounding with the retaining walls forms a potential risk of degrading the performance of seismically base-isolated buildings subjected to strong, especially near-fault, earthquake ground motions. Incremental dynamic analysis is employed to generate the so-called 'gap graph', in which two characteristic gap sizes of a base-isolated building are related with the isolation period of the building and the strength of the superstructure. The gap graph can be used to evaluate the required gap size for a base-isolated building to have certain collapse performance. This paper examines the interdependent relations of gap size with other factors that influence the seismic performance of the base-isolated building. Specifically, it is observed from the analysis results that near-fault pulse-like ground motions are likely to impose much higher demand for the isolation gap than far-field ones.

INTRODUCTION

Modern base isolation technique has been widely applied to residential and office buildings in Japan ever since the devastating 1995 M6.9 Kobe earthquake. During the same period of time, the technique has evolved and allows more flexible isolation layers so that the strength demand for superstructure can be further decreased. On the other hand, worries about the safety of base-isolated buildings subjected to strong earthquakes, especially near-fault motions, have arisen because a considerable part of them are located near major active faults. It is obvious that strong pulse-like near-fault motions are capable of subjecting flexible buildings to much greater displacement demand than expected (Hall *et al.*, 1995),

[a)] Structural Engineering Research Center, Tokyo Institute of Technology, Yokohama, 226-8503, Japan
[b)] Department of Architecture, Osaka Institute of Technology, Omiya, Asahi-ku, Osaka, 535-8585, Japan
[c)] Tokyo Kenchiku Co. Ltd., Shinanomachi, Shinjuku, Tokyo, 160-0016, Japan

which may subject the superstructure to impact against the surround retaining walls.

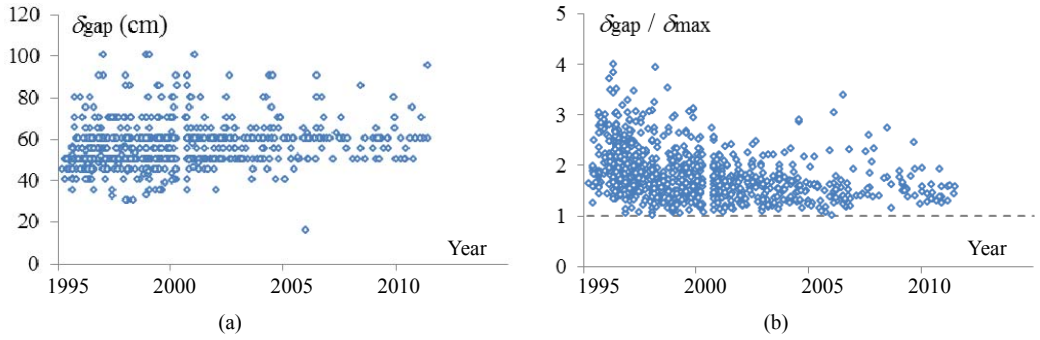

Figure 1. Statistics of isolation gap width of 979 seismically base-isolated buildings in Japan: (a) isolation gap width, δ_{gap} and (b) ratio of isolation gap width to maximum displacement, $\delta_{gap}/\delta_{max}$.

Even if incidents of significant pounding between base-isolated buildings and their retaining walls were not reported so far, Nagarajaiah and Sun (2001) presented a particular case that the base-isolated FCC building impacted against its entry bridge in the 1994 Northridge earthquake. Although it was attributed to the incorrect construction, rather than unexpected strong ground motion or inadequate isolation gap, this incident raised questions about the proportioning of the isolation gap, which is the most significant design parameter that addresses the risk of pounding, and it seems that rational methods have not yet been developed and implemented. Gap size, δ_{gap}, is generally considered adequate as long as it is no less than the total maximum displacement at isolation layer, δ_{max}, which is usually determined through nonlinear time history analysis or equivalent linear analysis of the base-isolated building of interest. In design practice, engineers are left quite arbitrary rather than rational in dealing with such a criterion. Figure 1 plots the isolation gap size of 979 base-isolated buildings constructed in Japan from 1995 to 2012. It seems that 60 cm gap size is gradually becoming an empirical standard regardless of δ_{max} as long as $\delta_{gap} \geq \delta_{max}$ is satisfied. On the other hand, the decision of δ_{gap} / δ_{max} ratio is subject to significant uncertainty and the engineers, probably encouraged by the aforementioned fact, tend to select smaller δ_{gap} / δ_{max} ratio in recent years, without evaluating the risk of pounding at base mat in future earthquakes.

A significant effect of the impact between the base mat of the superstructure and its surrounding retaining walls is that higher vibration mode of the superstructure will be excited

by the traveling of the impact energy along the height of the superstructure, resulting in much greater acceleration response and thus higher shear demand for the superstructure. This effect and the influence of various parameters, such as type of isolators, isolation gap width, retaining wall stiffness and impact model, has been investigated through numerical studies with uniform elastic shear beam models (Malhotra (1997)) or lumped mass elastic shear spring models (Matsagar and Jangid (2003), Komodromos *et al.* (2007)).

The higher than expected shear demand is very likely to push the superstructure of a base-isolated building far beyond its elastic limit. This may even eliminate the advantage of base-isolated buildings over conventional fixed base ones (Hall *et al.*, 1995). It is worth noting that the superstructure of a base-isolated building is elastically designed and is not seismically detailed for ductility from the very beginning of the development of modern base isolation technique in Japan. The exceedance of elastic limit may immediately trigger collapse of the superstructure. It is also significant to notice that the inelastic deformation of the superstructure tends to concentrate at the lower stories when the superstructure is subjected to pounding at its base mat (Tsai, 1997). This observation is confirmed by Pant and Wijeyewickrema (2012) in their analysis with more sophisticated inelastic frame model and also by Wang *et al.* (2006) in their hybrid test on an 8-story base-isolated building model. Such soft story behavior is unfavorable for the seismic performance of base-isolated buildings.

In this paper, the influence of gap size on the collapse performance of base-isolated multistory buildings is evaluated through extensive incremental dynamic analysis. Two characteristic gap sizes of a base-isolated building are defined based on the analysis results. Their dependence on various structural parameters as well as ground motion characteristics is investigated by means of the so-called ‘gap graph’, which can itself assist in choosing the gap size in the design practice of base-isolated buildings.

COLLAPSE PERFORMANCE OF BASE-ISOLATED BUILDINGS

Following the proposed methodology of determining the collapse performance of building structures in FEMA P695 (FEMA, 2009), the incremental dynamic analysis (IDA)

suggested by Vamvatsikos and Cornell (2002, 2004) is used to evaluate the probability of exceeding an assumed collapse limit-state for base-isolated buildings. In IDA, the seismic response of a building to a set of earthquake ground motions, which are scaled incrementally by an intensity measure (IM), is calculated through nonlinear dynamic analysis, and the fragility curve which relates IM to the probability of exceedance can be obtained. The IM that produces 50% probability of exceedance is then the median collapse capacity of the building corresponding to the assumed collapse limit-state. In order to allow for parametric study, a simple two degrees-of-freedom (DOF) lumped mass model is adopted in this study. The two DOFs are connected by two springs, one representing the isolation layer and the other the superstructure. The use of a single DOF to represent the superstructure imposes a major limitation that the effect of higher vibration mode, a major consequence of impact in base-isolated buildings, cannot be included in this study. However, a single DOF model is adequate to simulate the inelastic behavior of a multistory building exhibiting soft story mechanism, which is, as mentioned above, most common in base-isolated buildings subjected to pounding at the base.

The ductility factor μ of the superstructure, which is the ratio of the maximum to the yield lateral drift of the superstructure, is used to define the collapse limit-state. Two extreme cases for the ductility capacity of superstructures are considered here: (1) non-ductile case, in which the superstructure is assumed to collapse as long as its strength is reached, that is, when $\mu = 1$, and (2) ductile case, in which the superstructure is assumed to be seismically detailed to sustain very large plastic deformation. There is not yet consensus on ultimate ductility of structures within the research community, partly because of the various definitions of yield and ultimate displacement. For simplicity, $\mu = 8$ is taken herein as the collapse limit-state criterion for ductile RC superstructures. As suggested by Priestley et al. (2007), the yield drift of RC moment-resisting frames is of the order of 1/100. As a result, ductility of eight would result in 1/12.5 ultimate story drift, which is usually large enough to cause dynamic instability for RC structures.

It is worth noting that non-ductile superstructure is very common in the practical design of seismically isolated buildings in Japan, although it has long been excluded by related laws

in Japan for fixed-base earthquake-resistant buildings.

ANALYSIS MODEL

The 2DOF model is illustrated in Figure 1. The lower lumped mass, m_0, represents the mass of the base and the upper one, m_1, represents that of the rest of the superstructure. The superstructure is assumed to exhibit trilinear peak-oriented hysteretic behavior as shown in Figure 2(a), where F and Δ are the shear force and lateral deformation of the superstructure, respectively. The hysteretic rules follow the suggestion of Takeda et al. (1970).

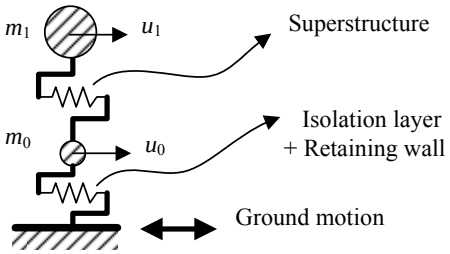

Figure 1. Lumped mass shear model

The isolation layer is assumed to consist of natural rubber bearings (NRBs) and hysteretic dampers. The trilinear elastic model suggested by Nakazawa et al. (2011) is adopted for modeling NRB (see Figure 2(b), where F and ε are the shear force and the shear strain of the rubber bearings, respectively). By calibrating with existing test data on NRBs subjected to large shear strain, they proposed that the bearing begins to exhibit strain hardening at 250% shear strain and the tangent stiffness becomes 2 times the initial stiffness, k_i, and then it further increases to $7k_i$ beyond 350% shear strain. Furthermore, the bearing fractures at 450% shear strain. The post-fracture behavior of the bearing is not modeled in this study. Instead, a large stiffness is assigned to the bearing when it exceeds 450% shear strain. The hysteretic dampers are modeled by an elastic-perfectly plastic spring and the retaining wall by a linear elastic spring with stiffness k_w and initial gaps on both sides of the origin (see Figure 2(c), where F and Δ are the reaction force of the retaining wall and the deformation of the isolation layer, respectively). The natural vibration period of the fixed-base superstructure, $T_f = 2\pi\sqrt{(m_1/K_0)}$, is assumed to be 0.3 s, representing typical short period multi-story RC buildings. The inherent damping of the building is assumed 2% of the critical damping. Among all the other parameters to fully define the structure, the following

five are to be investigated.

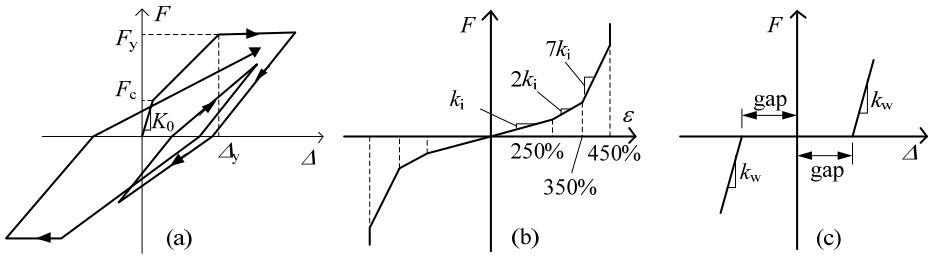

Figure 2. Hysteretic models for the base-isolated building: (a) superstructure, (b) natural rubber bearing and (c) retaining wall.

(1) The isolation period, T_i, which is defined as the period of the isolator (the NBR) and superstructure system, and is calculated by Equation (1). It neglects the stiffness of the dampers and assumes the superstructure to be rigid. It is considered one of the most important parameters in evaluating the effectiveness of seismic base-isolation. It is commonly higher than 3.5 s in the design practice in Japan (Pan et al., 2005).

$$T_i = 2\pi\sqrt{\frac{m}{k_i}} \tag{1}$$

where $m = m_0 + m_1$, is the total mass of the building and k_i is the initial stiffness of the isolators.

(2) The base shear coefficient, C_0, which is the ratio of the shear strength to the weight of the superstructure, that is, $C_0 = F_y / (m_1 g)$, where F_y is the shear strength (see Figure 2(a)) and g is the gravity acceleration. The required C_0 for multistory fixed-base RC buildings is generally greater than 0.3 in Japan. However, much smaller C_0 has been frequently used for the superstructure of base-isolated buildings. As reported by AIJ (2001), over 90% of the base-isolated buildings by the year of 2000 were designed with C_0 equal to or less than 0.15.

(3) The damper strength ratio, α_s, which is the ratio of the total yield strength of the dampers to the total weight of the structure. It is usually in the range of 0.03 to 0.05 (Pan et al., 2005).

(4) The retaining wall period, T_w, which is the period of the retaining wall and superstructure system, assuming the superstructure is rigid and neglecting the mass of the retaining wall. Similar to the isolation period T_i, it is calculated by Equation (2). It is merely a

measure of the retaining wall stiffness, which is believed important for the impact response of the base-isolated building.

$$T_w = 2\pi\sqrt{\frac{m}{k_w}} \tag{2}$$

where $m = m_0 + m_1$, is the total mass of the building and k_w is the stiffness of the retaining wall.

(5) The total rubber thickness of NRB, nt_R, which is directly related to the limit deformations at which the bearings begin to exhibit strain hardening and to fracture. n is the number of rubber layers and t_R is the thickness of a single rubber layer. The common value of nt_R is in the range of 120mm to 250mm in the engineering practice in Japan.

There are still several other parameters that cannot be derived from the above five. Among them, the gap size is the major parameter to be discussed later and some assumptions are made upon the others. For the trilinear hysteresis of the superstructure, it is assumed that the cracking strength, F_c, is one third of the yield strength, F_y, that the secant stiffness at the yield point is 0.3 times the initial stiffness, that the post yield stiffness ratio is 0.001 and that the unloading stiffness ratio that was defined by Takeda et al. (1970) is 0.4. In addition, the base mass, m_0, is assumed one fifth of m_1. The yield deformation of the hysteretic dampers is assumed to be 30 mm, a small value as compared to the expected displacement of the isolation layer.

GROUND MOTION RECORDS

Two ground motion record sets, a far-field and a near-field set, are composed for the incremental dynamic analysis. All the records are selected from the PEER ground motion database (PEER, 2012) and rules similar to those used in FEMA P695 report (FEMA, 2009) are followed in selecting the records except that (1) the valid frequency content is limited to at least 6 s to be applicable for the evaluation of base-isolated buildings with very long period of vibration and (2) the maximum number of records per event is increased to three to allow for more records for the analysis. In addition, the records in the far-field set should contain no pulse in both the two horizontal components while those in the near-field set should contain a pulse in at least one or both the two horizontal components and only the component

containing a pulse is used in the analysis. Whether a record component contains a pulse or not is based on the judgment of the latest version of the PEER database. As a result, 18 records with 36 non-pulse-like horizontal components and 22 records with 31 pulse-like horizontal components are selected for the far-field and the near-field set, respectively. Details of these records are given in the appendix.

As the analysis model is two dimensional, the two components of each record are normalized and used independently. Individual components are normalized by their respective peak ground velocities (PGVs) to the median of all their PGVs. The two sets are normalized separately. It is obvious from the median velocity spectra S_v in Figure 3 that the medium- and long-period component of the near-field set is much more significant than the ones of the far-field set while the short-period components of the two sets are close to each other after normalization.

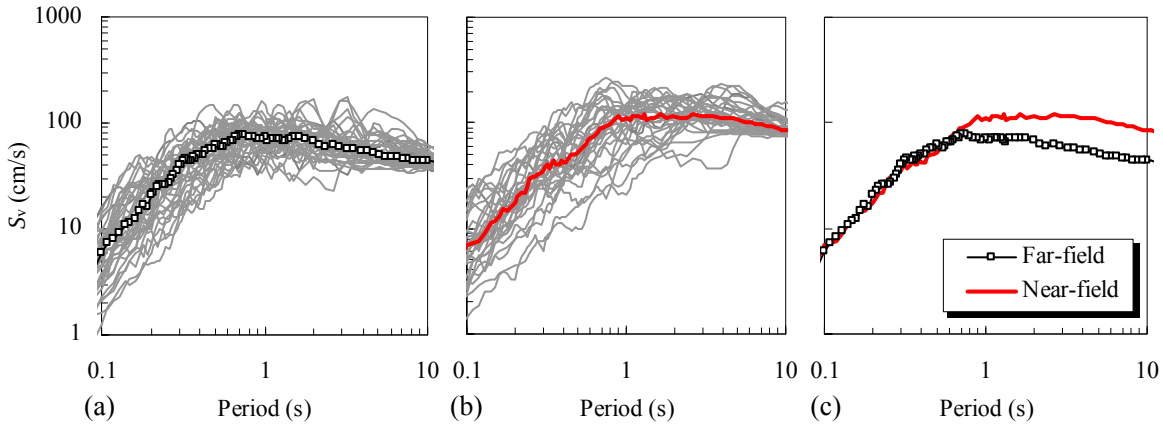

Figure 3. Spectral velocities of normalized ground motions (5% damping): (a) far-field set; (b) near-field set and (c) medians of the two sets

In IDA, the normalized set of ground motions is collectively scaled by some intensity measure (IM). The energy equivalent velocity at the isolation period, $V_E(T_i)$, is adopted herein as the IM. It is the velocity which makes the kinematic energy of the total mass of a system of natural period T_i equals the input energy, E_I, to the system under the ground motion. It has been widely used in Japan as a basis for the design of base-isolated buildings (AIJ, 2000).

The input energy, E_I, is calculated by Equation (3) (Akiyama, 1985), which is also referred to as the 'relative input energy' because it neglects the effort of the rigid body motion

of the building (Uang and Bertero, 1988). 10% damping ratio is assumed in calculating the input energy.

$$E_I = \int ma_g v dt \tag{3}$$

where a_g is the ground acceleration and v is the relative velocity of the mass.

The input energy, E_I, can be easily converted to V_E by Equation (4). One of the advantages of using V_E as the IM instead of E_I is that it has the unit of velocity and thus keeps linearly proportional to other commonly used IMs such as the spectral acceleration.

$$V_E = \sqrt{\frac{2E_I}{m}} \tag{4}$$

Figure 4 compares the median V_E spectra of the two ground motion sets after being scaled to $V_E(4\text{ s}) = 165.4$ cm/s. The selection of this velocity value will be explained later. The spectra within the range of period greater than about 2.5 s are very close to each other while the spectrum of the far-field set is much greater than that of the near-field set for shorter period.

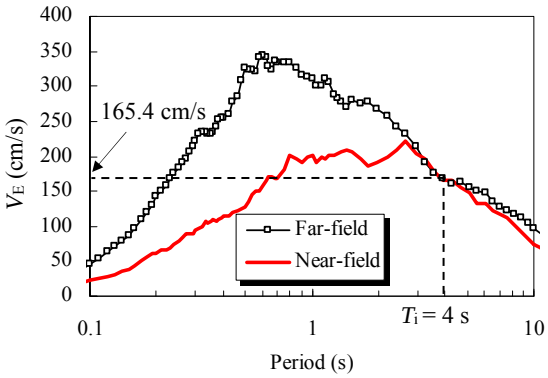

Figure 4. Median V_E spectra of the two sets scaled to $V_E(4\text{ s}) = 165.4$ cm/s (10% damping)

EVALUATION OF MEDIAN COLLAPSE CAPACITY

In IDA, each normalized ground motion is scaled starting from a scale factor of 0.1, and the "hunt & fill" algorithm (Vamvatsikos and Cornell, 2002) is adopted to search for the scale factor with which the assumed collapse limit-state (expressed by the ductility factor of the superstructure, μ, herein) is about to be reached. The required resolution for this target scale factor, that is, the difference between the target scale factor and the consequential one which

causes the building to exceed the limit-state, is set to be 0.05. The thus-obtained scale factor can then be converted to the intensity measure $V_E(T_i)$ by simply having it multiplied by the median $V_E(T_i)$ of the normalized, but un-scaled, ground motion set.

Thus $V_E(T_i)$ at the assumed limit-state can be found for each ground motions in the set. By assuming a log-normal distribution for $V_E(T_i)$ of all the ground motions, the $V_E(T_i)$ corresponding to 50% probability of exceeding the collapse limit-state can be found and is taken as the median collapse capacity, V_{EC}. Figure 5 demonstrates the above process of evaluating the capacity, which shows the IDA curves of the far-field set for ductile superstructure. The hollow box on each IDA curve indicates the target point obtained by the 'hunt & fill' algorithm. The ductile median collapse capacity, V_{EC}, indicated by the solid circle is read from the lognormal distribution curve at 50% probability of exceedance.

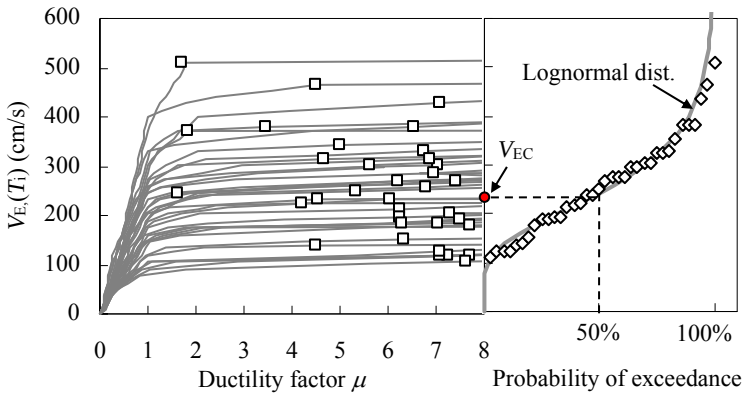

Figure 5. Median collapse capacity of ductile base-isolated building with $C_0 = 0.15$, $T_i = 4$ s, $\alpha_s = 0.04$, $T_w = T_f$, $nt_R = 200$ mm and gap size = 500 mm under far-field set.

CHARACTERISTIC GAP SIZES

RELATIONSHIP OF GAP SIZE VERSUS MEDIAN COLLAPSE CAPACITY

A change in any of the structural parameters described above will have more or less an influence on V_{EC} of a base-isolated building. Particularly, the influence of the gap size is of great interest of the present paper. It is expected that the increase of gap size would substantially increase the collapse capacity by reducing both the possibility of impact with the retaining wall and the impact velocity, if the impact does occur. To give an example, Figure 6 depicts the relationship of the gap size versus the median collapse capacity of base-isolated buildings of C_0 from 0.1 to 0.35, $T_i = 4$ s, $\alpha_s = 0.04$, $T_w = T_f$, $nt_R = 200$ mm,

subject to the far-field set ground motions. The results for both non-ductile and ductile cases are demonstrated. Almost linear relationship between the gap size and V_{EC} can be observed until a certain threshold size, beyond which the gap size has no more influence on the capacity. It is seen that C_0 has a great influence on the value of the threshold gap size. It has also significant effect on V_{EC} of ductile system when the gap size is less than the threshold. It is, however, quite reverse for the non-ductile cases.

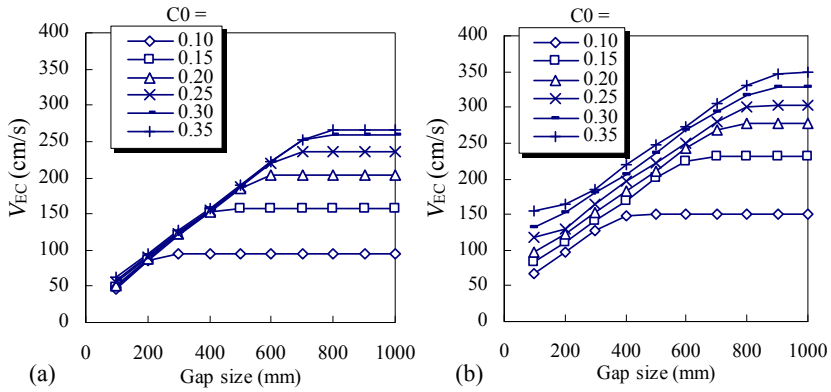

Figure 6. Influence of gap size on limit-state capacity (T_i = 4 s, α_s = 0.04, $T_w = T_f$, nt_R = 200 mm, far-field set): (a) non-ductile cases and (b) ductile cases

CHARACTERISTIC GAP SIZES

Based on the above observation, the gap size versus median collapse capacity relationship obtained by the analysis is fitted into two straight lines; a horizontal line representing the portion when the gap size has no more influence and an ascending one representing the rest portion. The intersection of these two straight lines is referred to as the maximum gap size, δ_{max}, hereafter. If a base-isolated building is provided with an isolation gap wider than δ_{max}, its collapse would have nothing to do with the collision with the retaining wall.

δ_{max} is sometimes too great to be practical for some applications because of the limited site area or some other economic considerations. In such cases, isolation gaps narrower than δ_{max} should be allowed and hence the impact with the retaining walls should be considered a source of deterioration of the performance of the base-isolated building in the design. However, the collapse performance should by no means be degraded to be worse than some minimum requirement, for example, the median collapse capacity, V_{EC}, should by no means be less than some minimum energy-equivalent velocity demand, V_{ED}. According to this, the gap size corresponding to V_{ED} on the fitted straight line is referred to as the minimum

required gap size, δ_{min} (Figure 7(a)). It represents a criterion where the collapse margin ratio is unity, that is, V_{EC} equals V_{ED}.

As far as the collapse performance is concerned, the minimum demand, V_{ED}, can be determined based on the Level II, that is, the maximum considered intensity level, energy spectrum suggested by BCJ (2006) for buildings on firm site (soil type II). The suggested energy spectrum is expressed in terms of energy-equivalent velocity and is obtained by simply dividing the design spectral acceleration, which is stipulated in the Building Standard Law of Japan (BCJ, 2004), by the circular vibration frequency of the building. Because the stipulated design spectral acceleration in the medium- and long-period range is proportional to the vibration frequency, the corresponding energy spectrum is constant in the medium- and long-period range. For firm sites (soil type II), it is constant at 165.4 cm/s for periods greater than 0.87 s.

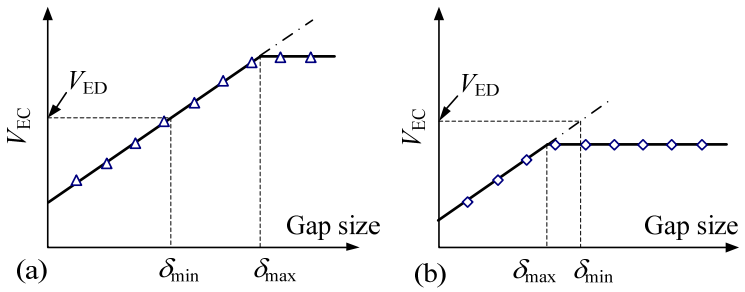

Figure 7. Characteristic gap sizes of base-isolated building: (a) when δ_{min} is less than δ_{max} and (b) when δ_{min} is greater than δ_{max}

By their physical meaning, the maximum gap size, δ_{max}, should always be no less than δ_{min}. However, it is possible that δ_{min} goes even greater than δ_{max} if it is determined from the fitted straight lines of the analysis results, no matter if from the part within the data range or from that beyond it (Figure 7(b)). This simply means that the studied base-isolated building cannot meet the requirement even if it has infinite isolation gap, or in other words, even if pounding is not taken into account. In this case, the design of the base-isolated building itself, rather than the selection of appropriate isolation gap size, should be carefully revised. In other cases, the two characteristic gap sizes, δ_{max} and δ_{min}, present the upper and lower bound for appropriate gap size. It is not economical if the gap size exceeds δ_{max}; on the other hand, it is not safe if the gap size is less than δ_{min}. In practical design, the lower bound, δ_{min}, is usually more useful. It ensures that isolated buildings sustain uniform collapse performance (in terms of energy-equivalent velocity) like other types of buildings even if major earthquakes subject isolated buildings to pounding incidents.

GAP GRAPH

FORMATION

The two characteristic gap sizes, δ_{max} and δ_{min}, and two of the major influential parameters, the isolation period, T_i, and the base shear coefficient, C_0, are integrated into a single graph, referred to as the 'gap graph'. It is a convenient tool in studying the interdependence of the two characteristic gap sizes and various parameters. The horizontal and the vertical axis of a gap graph are δ_{min} and δ_{max}, respectively. A pair of δ_{min} and δ_{max} forms a data point on the graph. Such points corresponding to base-isolated buildings of various C_0 and T_i are plotted and connected to form a net. A straight line starting from the origin representing $\delta_{min} = \delta_{max}$ is also plotted on the graph. Any data point falling below this line, that is, δ_{min} is greater than δ_{max}, indicates that the design of the base-isolated building requires revision. Figure 8 gives an example of the gap graph for base-isolated buildings with ductile superstructures and $\alpha_s = 0.04$, $T_w = T_f$, $nt_R = 200$ mm, subjected to the far-field ground motion set. The point of $C_0 = 0.1$, $T_i = 3.5$ s and $T_i = 4.0$ s falls below the diagonal line of $\delta_{min} = \delta_{max}$, indicating that these combinations of C_0 and T_i are not adequate to meet the capacity demand even if the isolation gap is infinite. Both δ_{min} and δ_{min} generally increase with the increase of the isolation period T_i, indicating that wider gaps should be provided for more flexible isolation systems. On the other hand, δ_{max} increases with the increase of C_0 while δ_{min}, on the contrary, decreases rapidly with it. This indicates that the disadvantage of using narrower isolation gap can be compensated by increasing the strength of the superstructure as far as the superstructure is ductile. To be noted that it is quite reverse if the non-ductile cases are concerned. This will be shown later.

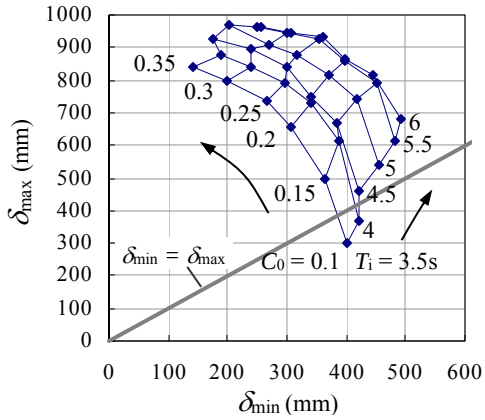

Figure 8. Gap graph of ductile base-isolated buildings with $\alpha_s = 0.04$, $T_w = T_f$ under far-field set

GAP GRAPHS WITH VARIOUS AMOUNTS OF DAMPERS

The gap graphs may serve as guidance for engineers in determining the size of the isolation gap of a base-isolated building in their design. A spectrum of gap graphs covering major parameters of a base-isolated system, for both non-ductile and ductile cases and subjected to both far-field and near-field ground motion sets, is provided in Figure 9. It is worth emphasizing that these results should only be used as only rough estimates and with full awareness of the assumptions and limitations upon which they are obtained. As the same as in Figure 8, each of the gap graphs covers the range of $C_0 = 0.10$ to 0.35 from bottom to upper part and $T_i = 3.5$ s to 6 s from left to right.

Besides C_0 and T_i, which are inherently included in a gap graph, the structural parameter recognized in Figure 9 is the amount of hysteretic dampers in the isolation layer in terms of α_s. The other important parameters, T_w and nt_R, are fixed at $T_w = T_f$ and $nt_R = 200$ mm in Figure 9. Their effect on the gap graph will be discussed later. The following observations can be made:

(1) As already shown in Figure 8, δ_{min} decreases rapidly with stronger superstructures, that is, greater C_0 when the superstructure is ductile. On the contrary, C_0 has little effect in decreasing δ_{min} for non-ductile cases even if the superstructure is as strong as a fixed-based building, for example, $C_0 = 0.3$. This is true for buildings of various α_s and various T_i subjected to either far-field or near-field ground motions.

(2) Greater T_i requires greater δ_{min} for both the non-ductile and the ductile cases. In the

practical design of base-isolated buildings, greater T_i, which indicates a more flexible isolation layer, is usually favorable because it generally leads to lower strength demand for the superstructure and thus makes the design more economically attractive. However, the increased flexibility of the isolation layer and the consequent potential decrease in the strength of the superstructure impose much greater demand for the isolation gap by increasing d_{min}. In such a manner, the flexibility of the isolator and the size of the isolation gap may form kind of trade-off in the design of a base-isolated building.

(3) The increase of the amount of dampers in the isolation layer, or in other words, the value of α_s, may help reducing δ_{min}. For example, for a building of $C_0 = 0.15$, $T_i = 5$ s and subject to far-field motions, the corresponding points on the gap graphs are marked by hollow circles in Figure 9. The value of δ_{min} corresponding to non-ductile cases decreases from 559 mm when $\alpha_s = 0.02$, to 472 mm when $\alpha_s = 0.04$ and further to 439 mm when $\alpha_s = 0.06$. Similarly, δ_{min} corresponding to ductile cases decreases from 489 mm when $\alpha_s = 0.02$, to 419 mm when $\alpha_s = 0.04$ and further to 380 mm when $\alpha_s = 0.06$. To be noted that greater α_s would increase the strength demand for the superstructure. Again, it is a trade-off for the selection of the value of α_s.

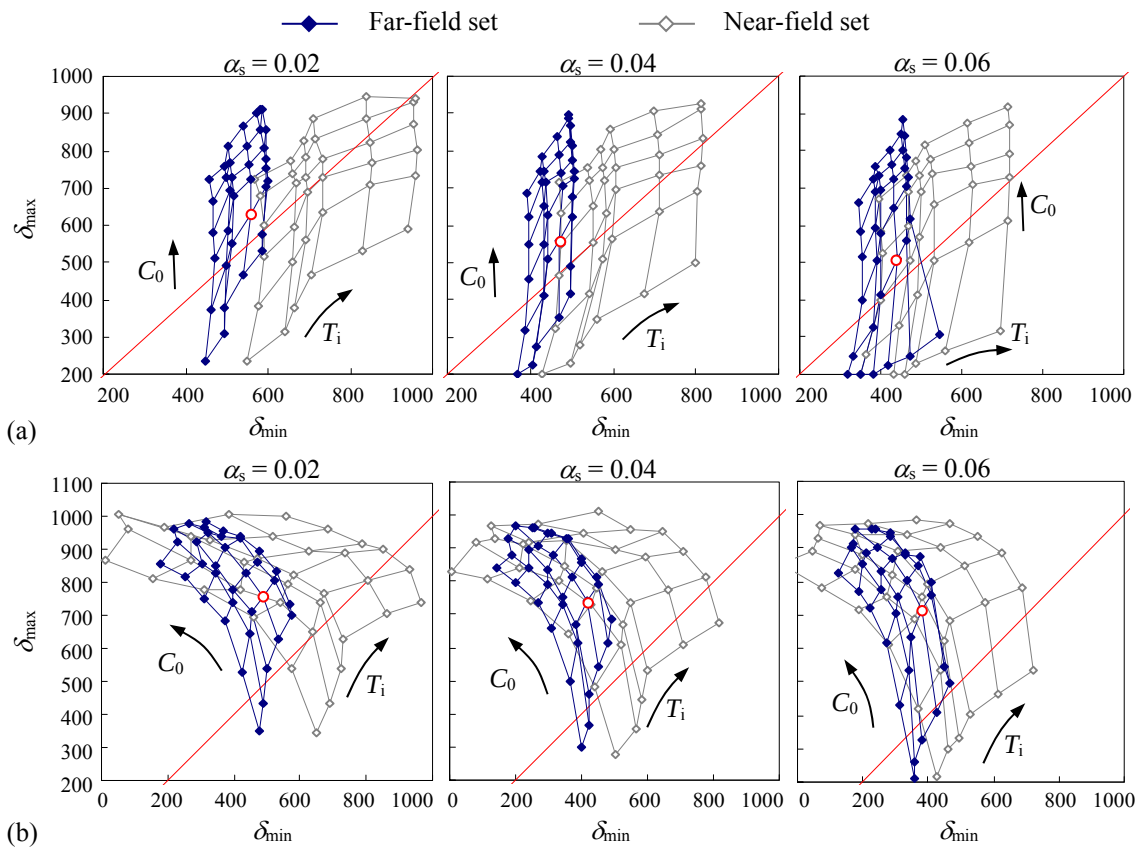

Figure 9. Gap graphs of base-isolated buildings with various amount of dampers subjected to either far-field or near-field motions ($T_w = T_f$, nt_R = 200mm): (a) non-ductile cases and (b) ductile cases.

(4) As mentioned above and as can be seen in Figure 4, the median V_E spectrum of the near-field set is generally smaller than that of the far-field set at the period equal to or less than T_i when they are scaled to the same IM. Notwithstanding this inferiority in response spectrum, the near-field set imposes much greater demand for δ_{min} than the far-field set. As far as the far-field set is concerned, 600 mm gap size, which is generally required and actually adopted in most base-isolated buildings in Japan, would be large enough to exceed δ_{min} of base-isolated buildings with moderate amount of dampers. However, it frequently becomes inadequate when the near-field set is used, especially for buildings of greater T_i and smaller C_0.

INFLUENCE OF RETAINING WALL STIFFNESS

The stiffness of the retaining wall comes from not only the retaining wall itself, which is usually made of reinforced concrete, but always from the soil backfill, too. A retaining wall with stiffness that makes T_w/T_f = 1 represents a quite practical case in the construction

practice of base-isolation system, although much smaller values of T_w/T_f ratio have been adopted by previous researchers. For example, it was assumed T_w/T_f = 0.29 by Tsai et al. (1997) and T_w/T_f in the range of 0.3~1.3 was investigated by Komodromos et al. (2007). To give a realistic example, an impact test was carried out on a real 5-story base-isolated reinforced concrete building in Japan before being demolished (Sano et al., 2010). The height of the building, h, is 21.85 m above the ground. The superstructure was about 2576 ton in weight and was isolated by 14 natural rubber bearings. The fixed-base period, T_f, of the building can be estimated empirically to be $0.02h$, that is, 0.437 s according to AIJ (2004). The reinforced concrete retaining wall is 200 mm thick and 1.2 m high. In the test, the superstructure was pulled back a certain distance by jacks and released suddenly to collide with the retaining wall. The measured stiffness of the retaining wall was 104.6 kN/mm, leading to a retaining wall period T_w = 0.986 s. Thus, the T_w / T_f ratio of this building is 2.2. Since this kind of test data is very limited and the stiffness of retaining wall is usually not considered in the design of base-isolated buildings, it seems appropriate to safely assume higher stiffness of retaining walls when considering the potential risk of pounding.

While the stiffness of retaining wall has much less effect on d_{max}, it would substantially decrease d_{min} when it becomes much lower. This effect is especially significant for stronger and ductile superstructures, as can be seen in Figure 10. For a building of C_0 = 0.15, T_i = 4s and subject to far-field ground motions, δ_{min} corresponding to non-ductile cases remains almost the same even if the retaining wall stiffness is reduced to one sixteenth (i.e., from T_w/T_f = 1 to T_w/T_f = 4). δ_{min} corresponding to ductile cases decreases from 406 mm at T_w/T_f = 0.5, to 386 mm at T_w/T_f = 1, 369 mm at T_w/T_f = 2 and 348 mm to T_w/T_f = 4. This difference becomes much more significant for buildings with stronger superstructures.

Although the cases of T_w/T_f = 8 seem unrealistically soft for an RC retaining wall, they are also depicted in Figure 10 to suggest the possibility of using some soft materials between the base of the superstructure and the retaining wall to allow a narrower isolation gap.

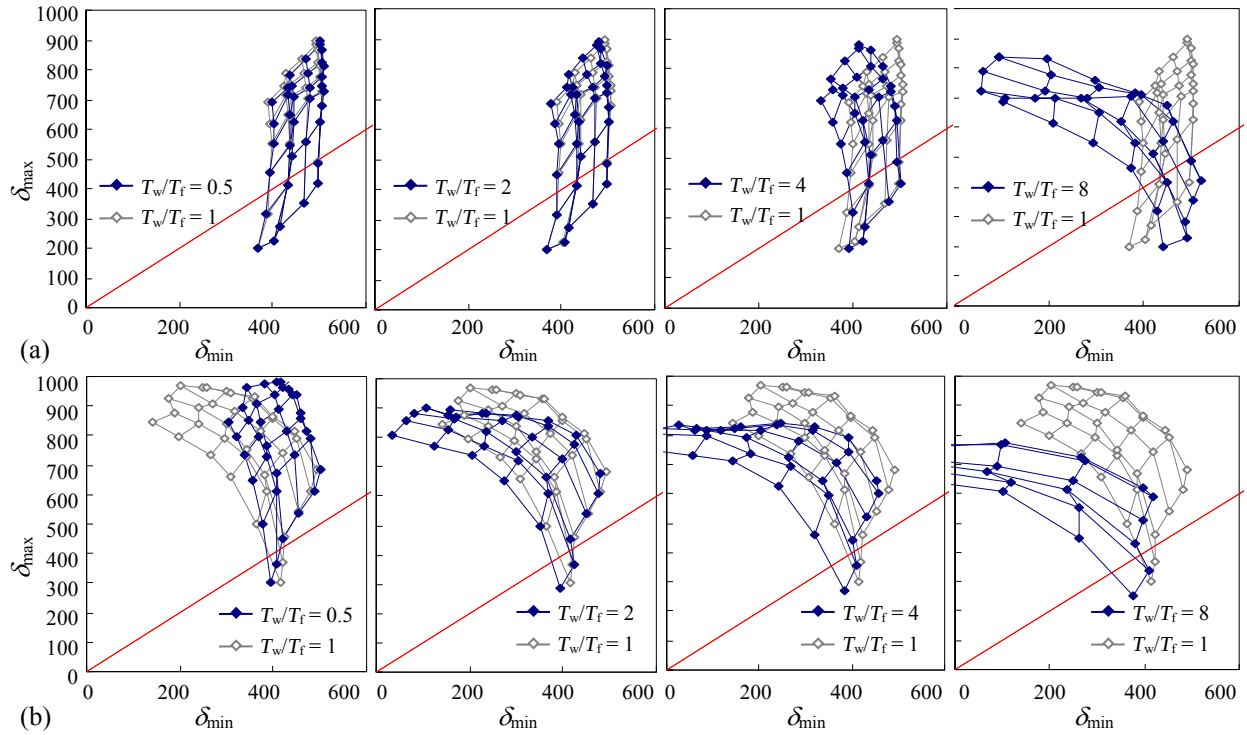

Figure 10. Influence of retaining walls stiffness on gap graphs (α_s = 0.04, nt_R = 200mm, Far-field set): (a) non-ductile limit-state and (b) ductile limit-state

INFLUENCE OF RUBBER THICKNESS

The total rubber thickness, nt_R, may also have some effect on the gap graph because it represents the limit deformation at which the bearing begins to exhibit strain hardening. The analysis results show that it has little effect on δ_{min} while it does have considerable influence on δ_{max} (Figure 11).

The effect of nt_R on δ_{max} can be easily estimated by a simple model without conducting any dynamic analysis. As already mentioned before, δ_{max} has the physical meaning that the failure of the superstructure would have nothing to do with the pounding if the gap size is greater than it. Instead, it should be due to the excessive shear force that is carried by the isolation layer and is transmitted to the superstructure when the rubber bearings are subjected to large deformation. Thus, it is natural to look for a shear deformation of the isolation layer, at which the shear force of the isolation layer equals the strength of the superstructure, and to make this deformation an estimation for δ_{max} of the building. This process is demonstrated in Figure 12 and the thus-obtained deformation is denoted as δ_{cal}. This method can be easily carried out as long as the restoring force versus deformation relationship of the isolation layer

is known. In this method, the influence of α_s, nt_R and C_0 on δ_{max} is taken into account. δ_{cal} obtained by this method and δ_{max} by the above analysis for buildings of various properties subject to both far-field and near-field motions are compared in Figure 13. For non-ductile cases, δ_{cal} is practically equal to δ_{max} for all the cases. For ductile cases, however, δ_{cal} is generally less than δ_{max}. It is probably due to the effect of the energy dissipation of the superstructure, which is not considered in the simple method of obtaining δ_{cal}. As shown in Figure 13(b), (δ_{cal} + 300 mm) provides a practical estimate for the upper bound of the δ_{max}.

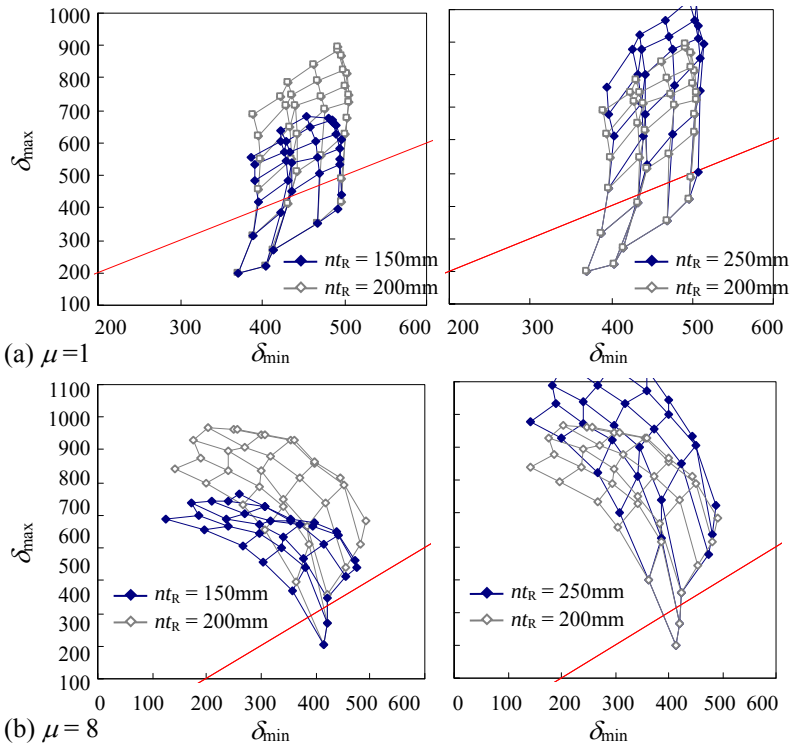

Figure 11. Influence of rubber thickness on gap graphs (α_s = 0.04, $T_w = T_f$, Far-field set): (a) non-ductile limit-state (μ = 1) and (b) ductile limit-state (μ = 8)

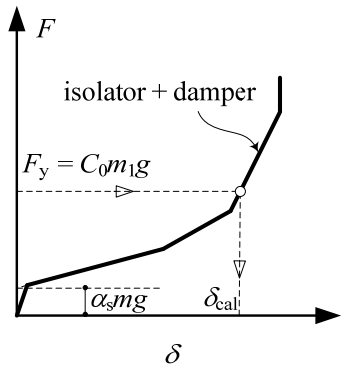

Figure 12. Model of calculating δ_{cal} as an estimate of δ_{max}

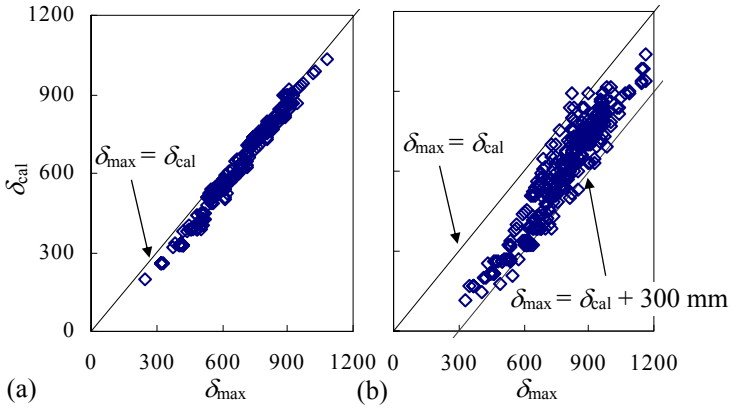

Figure 13. Relationship of δ_{max} versus δ_{cal}: (a) non-ductile limit-state and (b) ductile limit-state

CONCLUSIONS

Two characteristic gap sizes, δ_{max} and δ_{min}, are defined in examining the influence of gap size on the collapse performance of seismically base-isolated buildings. By forming a gap graph, the dependence of these two characteristic gap sizes on major structural parameters of base-isolated buildings and ground motion characteristics is investigated. The following conclusions may be drawn from the above results and discussions.

(1) For isolated buildings with non-ductile superstructures, the demand for isolation gap size in terms of δ_{min} can be reduced either by increasing the amount of dampers in the isolation layers or by reducing significantly the stiffness of the retaining wall. At the same time, this demand would increase rapidly when the isolation layer gets more flexible. In addition, it seems not effective to reduce this demand by increasing the strength of the superstructure.

(2) For isolated buildings with ductile superstructures, the influence of major structural parameters on the demand for isolation gap size in terms of δ_{min} is similar to that for the non-ductile cases except that the increase of the superstructure strength would substantially reduce the demand for isolation gap size.

(3) The near-fault pulse-like ground motions may produce much greater δ_{min} than the far-field ones. For flexible isolation system, for example, T_i equals 5.5 s or even 6 s, a gap as wide as 600 mm, which is currently a common practice in Japan, may still fail to meet the demand in terms of δ_{min}. This suggests a potential risk for the many base-isolated buildings located close to major active faults.

(4) The maximum gap size, δ_{max}, represents a threshold whether the performance of the base-isolated building is influenced by pounding. It can be satisfactorily estimated by the proposed simple method for non-ductile cases.

It is worth noting that the above conclusions are based on analytical models with single-degree-of-freedom system as the superstructures. Accelerations of the superstructure, which are also of major concern for the seismic performance of base-isolated buildings, and which may be greatly influenced by impact of the isolation layer, are not discussed in this

paper. Although similar ideas could be followed to produce gap graphs corresponding to some acceleration limit-states, much more computational effort might be required because multi-degree-of-freedom models might become necessary for the superstructure to capture the higher vibrations mode.

REFERENCE

AIJ, 2001. *Recommendation for design of base isolated structures*. Architectural Institute of Japan, Tokyo. (In Japanese)

AIJ, 2004. *Recommendation for loads on buildings*. Architectural Institute of Japan, Tokyo: 453-454 (In Japanese)

Akiyama, H., 1985. *Earthquake-resistant limit-state design for buildings*, University of Tokyo Press, Tokyo: 11-12.

BCJ, 2004. *Building standard law of Japan*. Building Center of Japan, Tokyo (In Japanese)

BCJ, 2006. *Technical recommendation for energy-based earthquake-resistant limit-state design*. Building Center of Japan, Tokyo (In Japanese)

FEMA, 2009. *Quantification of building seismic performance factors*, Report No. FEMA P695.

Hall, J. F.; Heaton, T. H.; Halling, M. W.; Wald, D. I., 1995. Near-source ground motion and its effects on flexible buildings, *Earthquake Spectra*, **11**(4): 569-605.

Komodromos, P., Polycarpou, P. C., Papaloizou, L., Phocas, M. C., 2007. Response of seismically isolated buildings considering poundings, *Earthquake Engineering and Structural Dynamics*, **36**(12): 1605-1622.

Maeno, T., Yamamoto. S., Nakamura, N., Matsushima, S., Kawase, H., 2010. Shake table test of base-isolated buildings pounding against retaining wall, *Proc. Symposium on responses of buildings to pulse-like ground motions* Tokyo, Japan: 19-25.

Malhotra, P. K., 1997. Dynamics of seismic impacts in base-isolated buildings, *Earthquake Engineering and Structural Dynamics*, **26**(8): 797-813.

Matsagar, V. A., Jangid, R. S., 2003. Seismic response of base-isolated structures during impact with adjacent structures, *Engineering Structures*, **25**(10): 1311-1323.

Nagarajaiah, S., Sun, X., 2001. Base-isolated FCC Building: Impact response in Northridge earthquake. *Journal of Structural Engineering, ASCE*, **127**(9): 1063-1075.

Nakazawa, T., Kishiki, S., Qu, Z., Miyoshi, A., Wada, A., 2011. Fundamental study on probabilistic evaluation of ultimate state of base isolated structures, *Journal of Structural and Construction Engineering, Transaction of AIJ*, **76**: 745-754. (in Japanese)

Pan, P., Zamfirescu, D., Nakashima, M., Nariaki, N., Hisatoshi, K., 2005. Base-isolation design practice in Japan: Introduction to the post-Kobe approach, *Journal of Earthquake Engineering* **9**(1): 147-171.

Pant, D. R., Wijeyewickrema, A. C., 2012. Structural performance of a base-isolated reinforced concrete building subjected to seismic pounding, *Earthquake Engineering and Structural Dynamics*. DOI: 10.1002/eqe.2158

Priestley, M. J. N., Calvi, G. M., Kowalsky, M. J., 2007. Displacement-based seismic design of structures, IUSS Press, Pavia, Italy, 2007: 226.

PEER, 2012. PEER ground motion database, Pacific Earthquake Engineering Research Center. Available from: http://peer.berkeley.edu/peer_ground_motion_database [10 Dec 2011].

Sano, T., Miwada, G., Katsumata, H., Komaki, J., Sato, K., Takiyama, N., Hayashi, Y., 2010. Experiments of collision to retaining wall with real scale base-isolated building: Part 1~5, *Summaries of technical papers of AIJ annual meeting*, B-2: 427-436.

Takeda, T., Sozen, M. A., Nielson, N. N., 1970. Reinforced concrete response to simulated earthquakes, *Journal of Structural Division, ASCE*, **96**(12): 2557-2573.

Tsai, H. C., 1997. Dynamic analysis of base-isolated shear beams bumping against stops, *Earthquake Engineering and Structural Dynamics*, **26**(5): 515-528.

Uang, C. M., Bertero, V. V., 1988. Use of energy as a design criterion in earthquake-resistant design. Report No. UCB/EERC-88/18, University of California at Berkeley, CA: 5-6.

Vamvatsikos, D., Cornell, C. A., 2002. Incremental dynamic analysis, *Earthquake Engineering and Structural Dynamics*, **31**(3): 491-514.

Vamvatsikos, D., Cornell, C. A., 2004. Applied incremental dynamic analysis, *Earthquake spectra*, **20**(2): 523-553.

Wang, T.; Nakashima, M., Pan, P., 2006. On-line hybrid test combining with general-purpose finite element software, *Earthquake Engineering and Structural Dynamics*, **35**(2): 1471-1488.

Appendix:

Table A. Ground motion records in near-field set

ID	Earthquake Name	Mechanism	Fault Distance (km)	Shear wave velocity Vs30 (m/s)	Lowest usable frequency (Hz)	PGA (g)	PGV (cm/s)	PGA (g)	PGV (cm/s)
180	1979 Imperial Valley, US	Strike-slip	3.29	205.6	0.125	0.5191	46.84	0.3785	90.45
182	1979 Imperial Valley, US	Strike-slip	2.08	210.5	0.125	0.3375	47.56	0.4630	109.17
181	1979 Imperial Valley, US	Strike-slip	1.75	203.2	0.125	0.4105	64.80	0.4390	109.74
496	1985 Nahanni, Canada	Reverse	2.47	659.6	0.125	0.4890	29.23	0.3226	33.10
723	1987 Superstition Hills, US	Strike-slip	2.24	348.7	0.150	0.4550	111.89	0.3772	43.90
802	1989 Loma Prieta, US	Reverse	8.04	370.8	0.125	0.5125	41.12	0.3242	42.58
803	1989 Loma Prieta, US	Reverse	8.90	370.8	0.125	0.2551	42.41	0.3322	61.50
779	1989 Loma Prieta, US	Reverse	1.94	477.7	0.125	0.9663	108.57	0.5872	47.01
821	1992 Erzican, Turkey	Strike-slip	2.19	274.5	0.125	0.5153	83.88	0.4955	64.25
828	1992 Cape Mendocino, US	Reverse	4.09	712.8	0.070	0.5896	48.28	0.6624	90.07
825	1992 Cape Mendocino, US	Reverse	3.48	513.7	0.070	1.4973	125.38	1.0395	41.28
879	1992 Landers, US	Strike-slip	2.95	684.9	0.100	0.7268	146.62	0.7892	32.52
1044	1994 Northridge, US	Reverse	4.54	269.1	0.120	0.5830	75.76	0.5898	97.68
1086	1994 Northridge, US	Reverse	3.52	440.5	0.120	0.6045	78.25	0.8433	130.24
1063	1994 Northridge, US	Reverse	3.25	282.3	0.113	0.8252	160.16	0.4865	74.52
1106	1995 Kobe, Japan	Strike-slip	2.09	312.0	0.063	0.8213	81.55	0.5985	74.71
1176	1999 Kocaeli, Turkey	Strike-slip	3.35	297.0	0.088	0.2677	65.67	0.3490	62.12
1503	1999 Chi-Chi, Taiwan	Reverse	3.66	305.9	0.075	0.8138	126.09	0.6028	78.74
1492	1999 Chi-Chi, Taiwan	Reverse	2.50	579.1	0.050	0.3482	158.88	0.4190	118.39
1505	1999 Chi-Chi, Taiwan	Reverse	2.81	487.3	0.038	0.5660	176.49	0.4617	262.97
1605	1999 Duzce, Turkey	Strike-slip	3.30	276.0	0.100	0.3481	59.93	0.5353	83.43
2114	2001 Denali, US	Strike-slip	1.97	329.4	0.025	0.3190	134.63	0.3178	75.92

Shadowed components are excluded in the selection because they contain no pulse.

Table B. Ground motion records in far-field set

ID	Earthquake Name	Mechanism	Fault Distance (km)	Shear wave velocity Vs30 (m/s)	Lowest usable frequency (Hz)	PGA (g)	PGV (cm/s)	PGA (g)	PGV (cm/s)
125	1976 Friuli, Italy	Reverse	15.40	424.8	0.125	0.3513	22.02	0.3148	30.78
169	1979 Imperial Valley, US	Strike-slip	22.29	274.5	0.063	0.2378	25.98	0.3511	32.99
806	1989 Loma Prieta, US	Reverse	24.08	267.7	0.125	0.2073	37.24	0.2086	36.01
778	1989 Loma Prieta, US	Reverse	24.67	215.5	0.125	0.2687	43.84	0.2789	35.53
777	1989 Loma Prieta, US	Reverse	27.47	198.8	0.125	0.2465	38.46	0.2148	44.94
829	1992 Cape Mendocino, US	Reverse	11.11	311.8	0.070	0.3854	43.78	0.5489	42.04
848	1992 Landers, US	Strike-slip	19.86	271.4	0.125	0.2828	25.62	0.4169	42.30
864	1992 Landers, US	Strike-slip	11.23	379.3	0.070	0.2737	27.47	0.2840	43.36
1003	1994 Northridge-01	Reverse	24.09	308.7	0.125	0.4745	34.44	0.4386	39.11
960	1994 Northridge-01	Reverse	11.92	308.6	0.125	0.4100	42.98	0.4820	45.37
963	1994 Northridge-01	Reverse	20.41	450.3	0.120	0.5683	52.54	0.5143	52.17
1107	1995 Kobe, Japan	Strike-slip	22.84	312.0	0.125	0.2514	18.76	0.3447	27.64
1116	1995 Kobe, Japan	Strike-slip	19.38	256.0	0.125	0.2432	37.84	0.2119	27.92
1201	1999 Chi-Chi, Taiwan	Reverse	15.58	378.8	0.038	0.3097	48.47	0.2485	38.81
1524	1999 Chi-Chi, Taiwan	Reverse	45.22	446.6	0.050	0.3785	62.02	0.7116	49.14
1595	1999 Chi-Chi, Taiwan	Reverse	12.70	258.9	0.088	0.3338	69.01	0.4837	74.40
1633	1990 Manjil, Iran	Strike-slip	12.77	724.0	0.130	0.5146	43.21	0.4964	54.06
1787	1999 Hector Mine	Strike-slip	11.19	684.9	0.038	0.2656	28.56	0.3368	41.72